Exploiting the Synergetic Behavior of PtPd Bimetallic Catalysts in the Selective Hydrogenation of Glucose and Furfural

Priscilla de Souza, Lishil Silvester, Anderson da Silva, Cibele Fernandes, Thenner Rodrigues, Sébastien Paul, Pedro Camargo, Robert Wojcieszak

catalysts

MDPI

Article

Exploiting the Synergetic Behavior of PtPd Bimetallic Catalysts in the Selective Hydrogenation of Glucose and Furfural

Priscilla M. de Souza [1], Lishil Silvester [2], Anderson G. M. da Silva [3], Cibele G. Fernandes [3], Thenner S. Rodrigues [3], Sebastien Paul [2], Pedro H. C. Camargo [3] and Robert Wojcieszak [2,*]

1 Programa de Engenharia Química—COPPE, Universidade de Rio de Janeiro, Rio de Janeiro 21941–972, Brazil; magalhaesdesouza@gmail.com

2 University of Lille, CNRS, Centrale Lille, ENSCL, Univ. Artois, UMR 8181-UCCS-Unité de Catalyse et Chimie du Solide, F-59000 Lille, France; lishil.silvester@centralelille.fr (L.S.); sebastien.paul@centralelille.fr (S.P.)

3 Departamento de Química Fundamental, Instituto de Química, Universidade de São Paulo, Av. Prof. Lineu Prestes, 748, São Paulo-SP 05508-000, Brazil; andersondeob@gmail.com (A.G.M.d.S.); cibele.fernandes@iq.usp.br (C.G.F.); thenner07@yahoo.com.br (T.S.R.); camargo@iq.usp.br (P.H.C.C.)

* Correspondence: robert.wojcieszak@univ-lille.fr

Received: 27 December 2018; Accepted: 16 January 2019; Published: 1 February 2019

Abstract: Mono and bimetallic catalysts based on Pt and Pd were prepared by a co-precipitation method. They were tested in liquid phase hydrogenation reactions of glucose and furfural at low temperature and pressure. The bimetallic PtPd/TiO_2 catalyst proved to be an efficient material in selectively hydrogenating glucose to sorbitol. Moreover, high furfural conversion was attained under relatively soft conditions, and the furfuryl alcohol selectivity was strongly affected by the chemical composition of the catalysts. Furfuryl alcohol (FA) was the major product in most cases, along with side products such as methylfuran (MF), furan, and traces of tetrahydrofuran (THF). These results showed that the PtPd bimetallic sample was more active relative to the monometallic counterparts. A correlation between the catalytic results and the physicochemical properties of the supported nanoparticles identified key factors responsible for the synergetic behavior of the PtPd system. The high activity and selectivity were due to the formation of ultra-small particles, alloy formation, and the Pt-rich surface composition of the bimetallic particles supported on the TiO_2 nanowires.

Keywords: Pt; Pd; bimetallic; hydrogenation; sorbitol; furfural; X-ray photoelectron spectroscopy (XPS)

1. Introduction

In recent decades, the conversion of biomass raw materials to platform molecules has gained interest, as it is one of the most promising routes for the sustainable production of bio-fuels and bio-chemicals [1–5]. Furfural and glucose are considered as important biomass-derived compounds among the platform molecules, as they are the source of top most value-added chemicals like sorbitol and furfuryl alcohol, respectively [1,6,7]. Furfuryl alcohol is considered as a potential source to produce alkane components in liquid biofuels, and its derivatives have wide applications in the plastics, pharmaceuticals, food, and agrochemical industries [1,8–10]. Sorbitol is widely used in the cosmetics, food, and pharmaceutical industries, and is considered as an outstanding building block for commodity chemicals such as isosorbide and sorbitan [4,5,7,11]. It has been estimated that more than

60% of the overall furfural produced each year is converted to furfuryl alcohol, whereas the majority of the globally produced sorbitol (~700,000 tons/year) is obtained from glucose [4,7,12].

Various heterogeneous catalysts, mainly based on Ni, Cu, Ru, Pd, and Pt, have been studied in the selective hydrogenations of glucose [4,5,11,13–19] and furfural [3,20–32]. In glucose hydrogenation reactions, nickel- and ruthenium-based catalytic systems are commercially favored because of their excellent activities in addition to their lower costs compared to other noble metal catalysts. However, the Ni catalysts exhibit deactivation due to metal leaching, sintering, and active site poisoning, and the Ru catalysts, in addition to their high cost, show deactivation resulting from agglomeration/sintering, metal migration, and poisoning from organic by-products [4,5,11,13,19,33,34]. In the case of furfural hydrogenation, copper-chromite and Ni-based catalysts are widely employed due to their selective nature and low cost compared to noble metal catalysts. However, they possess some drawbacks, such as not being environmentally benign, deactivating due to chromium migration, poisoning by the by-products, leading to non-selective/total hydrogenation, and displaying poor recycling ability [2,3,21,23–25,32,35–37].

Due to the aforementioned limitations of the commonly used catalysts in glucose and furfural hydrogenation reactions, noble metal catalysts, mainly based on Pt and Pd, have been studied, as they are known to exhibit high activity, strong deactivation resistance, and regeneration ability in different catalytic reactions [38–40]. While the Pd catalytic systems have exhibited total conversion or C–C bond cleavage leading to unwanted products, the Pt catalysts have showed higher selectivity at comparatively lower conversions [17,19,41–43]. Hydrogenation of furfural performed using bimetallic PdFe and PdCu catalysts proved that the addition of a second metal to a Pd catalyst reduced the C–C cleavage and increased the selectivity to furfuryl alcohol [28,44]. Although PtPd bimetallic catalysts have been successfully employed in hydrogenation of various chemicals and are known to possess synergetic behavior [45–49], they have rarely been studied in both glucose and furfural hydrogenation reactions as per our knowledge [42,50]. For example, Albilali et al. used a PtPd bimetallic catalyst in furfural hydrogenation to screen for suitable conditions that yield more tetrahydrofurfuryl alcohol, a total hydrogenation product of furfural [50].

In addition to the active phase (noble-metal nanoparticle), the nature of the support of the catalysts is another factor that affects the product distributions in all catalytic systems. Among the commonly known SiO_2, Al_2O_3, TiO_2, and ZrO_2 supports, TiO_2-supported catalysts exhibit higher selectivity towards both sorbitol and furfuryl alcohol [51,52]. During the hydrogenation of furfural, TiO_2 facilitates the formation of the active furfuryl-oxy intermediate due to charge-transfer interactions between the furfural molecule and an O-vacancy site on the TiO_2 surface, resulting in enhanced furfuryl alcohol selectivity [52].

Based on the aforementioned challenges, we aim in this paper to exploit the synergetic effects of PtPd bimetallic nanocatalysts (relative to their monometallic Pd and Pt counterparts), towards the selective/partial hydrogenations of glucose and furfural to sorbitol and furfuryl alcohol, respectively. Our main focus was to understand the influence of synergetic behavior in well-defined and controlled PtPd bimetallic nanoparticles supported on TiO_2 nanowires as catalysts in selective hydrogenations of glucose and furfural.

2. Results and Discussion

2.1. Catalyst Characterization

XRD studies were performed in order to confirm the structure of the TiO_2 support and to detect the presence of any large metallic or bimetallic nanoparticles. As shown in Figure 1, no diffraction peaks assigned to metallic Pd or Pt were observed, most probably as a result of the formation of very small metallic nanoparticles (<3 nm NPs) on the TiO_2 nanowire surface. The diffractograms confirmed that the support TiO_2 mainly exists as anatase phase (noted as 'A' on Figure 1) in all catalysts. However,

a small contribution from the rutile phase (noted as 'R' on Figure 1) is also confirmed by a peak at $2\theta = 28°$.

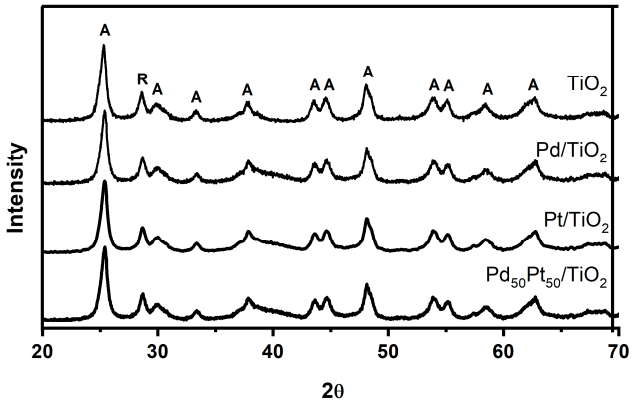

Figure 1. XRD patterns of the bare TiO_2 nanowires support and the TiO_2 nanowires support decorated with ultra-small Pd, Pt, and PtPd nanoparticles (NPs).

In order to confirm the presence of Pt and Pd nanoparticles that were not detected by XRD, transmission electron microscopy was performed. The images clearly showed that the TiO_2 support exists as nanowires in all catalysts, as shown in Figure 2A,B. TEM studies confirmed the formation of very small nanoparticles (NPs < 5 nm) of both Pt and Pd metals that are highly and homogeneously dispersed on the TiO_2 surface, as shown in Figure 2C,D. Furthermore, the high-resolution images (HRTEM) confirmed the presence of ultra-small Pt and Pd particles with an average size of about 2 nm, as illustrated in Figure 3. The formation of these highly dispersed ultra-small metallic particles is hence the reason for the absence of metallic Pt and Pd characteristic peaks in XRD.

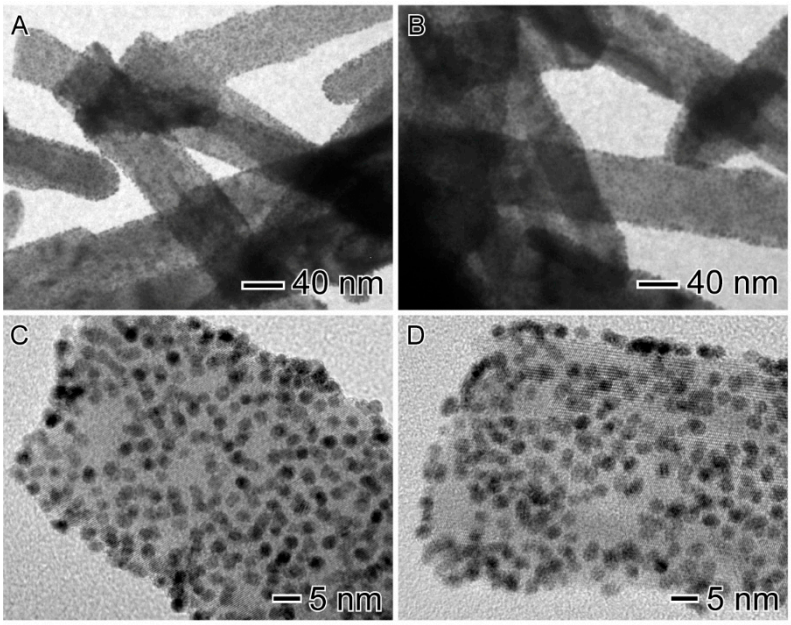

Figure 2. TEM (**A**,**B**) and HRTEM (**C**,**D**) images of TiO_2 nanowires decorated with ultrasmall Pd (**A** and **C**) and Pt (**B** and **D**) nanoparticles, covering the entire surface of the nanowires.

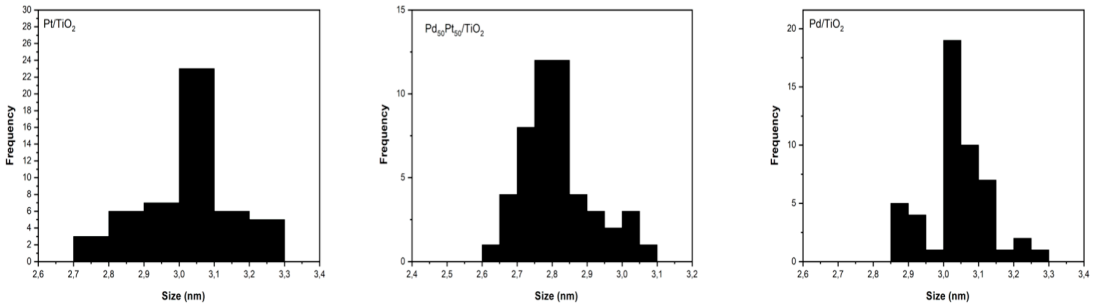

Figure 3. TEM particle size distribution of for mono and bimetallic samples.

TEM results also confirmed that the reduction–precipitation method used for the syntheses of all catalysts is adequate for the low surface area supports (<50 m^2 g^{-1}, Table 1) to obtain high dispersion of metallic nanoparticles without any agglomeration. Indeed, the most important problem when working with low surface area oxides is the control of the deposited metallic nanoparticles. It is already well established that a highly dispersed active phase (especially metallic phase) in the catalyst is necessary to enhance the catalytic activity and durability of metal-based materials [53]. Different methods can be applied [54,55] to obtain homogeneous dispersion of small metallic particles on the support surface, but generally the catalysts with well-dispersed particles are prepared by the traditional impregnation or precipitation methods. In this study, the chemical reduction with $NaBH_4$ in the presence of a stabilizer (polyvinyl alcohol—PVA) during catalyst syntheses permitted us to not only easily obtain zerovalent states in Pt and Pd metals, but also to stabilize particles on the surface of TiO_2 supports with low surface area.

Table 1. Brunauer-Emmett-Teller (BET) surface area and chemical composition of the samples determined by BET and FAAS.

Catalyst	(wt.%)		Surface Area (m^2 g^{-1})	Average Pore Diameter (Å)	Pore Volume (cm^3 g^{-1})
	Pt	Pd			
Pt/TiO_2	2.0	0.0	49	55.9	0.0902
$Pt_{0.50}Pd_{0.50}/TiO_2$	1.3	0.9	44	59.4	0.0804
Pd/TiO_2	0.0	2.3	33	64.4	0.0691
TiO_2	-	-	40		

TEM was also performed for bimetallic $Pt_{0.50}Pd_{0.50}$ catalysts in order to verify if there are any differences in particle size distributions or metal dispersion compared to monometallic catalysts due to the possible formation of alloys in the bimetallic catalyst. This is illustrated in Figure 3. There is no observable differences in particle sizes and dispersion of metallic particles in monometallic and bimetallic catalysts (2.7–3 nm). However, it is difficult to observe the minute differences in the structures of monometallic and bimetallic catalysts due to the presence of very small particle sizes, and so one cannot fully deny the formation of an alloy structure in $Pt_{50}Pd_{50}$ bimetallic catalysts merely by looking at TEM results.

Electronic interactions can occur in bimetallic $Pt_{0.50}Pd_{0.50}$ material, and they can modify the oxidation states of the metals, especially in the case of core-shell structures. For the bimetallic $Pt_{0.50}Pd_{0.50}$ sample, X-ray photoelectron spectroscopy (XPS) analysis showed the enrichment of Pt on the surface. The trends in the relative percentages of Pd^0 and Pt^0 in the bimetallic sample point out important differences in the interaction between these two metals. The formation of ultra-small Pt–Pd particles with a possible alloy structure was deduced from TEM study, as illustrated in Figure 4. Indeed, the binding energies of Pt^0 4f ($4f_{7/2}$ = 72.4 eV) and Pd^0 3d ($3d_{5/2}$ = 337.0 eV) are slightly different from the standard values of bulk Pt^0 ($4f_{7/2}$ = 71.30 eV) and bulk Pd^0 ($3d_{5/2}$ = 334.80 eV). These variations in the standard energy peak locations are due to the electronic interactions between the Pt and Pd within the particles. Moreover, the Pt 4f region also showed the existence of Pt^{2+} species

in the catalysts (about 25%). This is because the surfaces of Pt particles might have been oxidized during the preparation process. The lower intensity of the Pd 3d peak as compared to the Pt 3d peak suggests the existence of local Pt enrichment on the surfaces of nanoparticles in bimetallic catalysts.

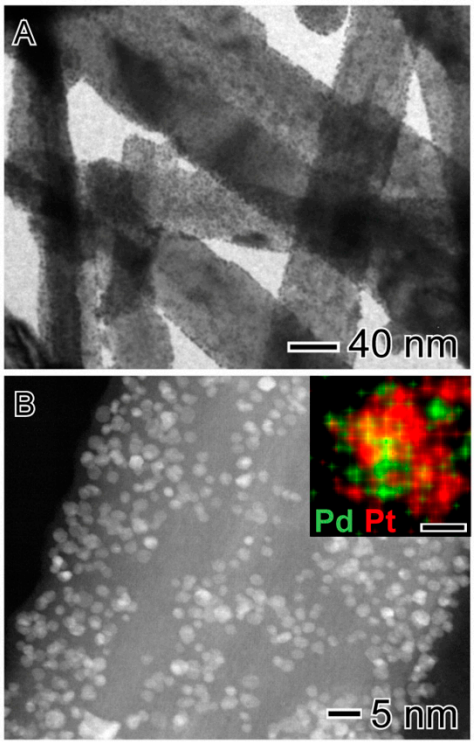

Figure 4. TEM (**A**) and STEM high-angle annular dark field (HAADF) (**B**) images of TiO_2 nanowires decorated with ultra-small bimetallic PtPd NPs. The image inset in **B** shows a STEM-EDX elemental map for a single PtPd nanoparticle at the surface of TiO_2 nanowires.

Concerning the O 1s XPS region, three different surface oxygen species were identified, namely, lattice oxygen (O_L), surface oxygen ions (O_S), and oxygen originating from adsorbed species such as water and organic carbon (O_W). Binding energies and atomic percentages of all types of oxygen are reported in Table 2.

Table 2. Binding energies and surface metallic compositions for the TiO_2 nanowires decorated with ultra-small Pt, PtPd, and Pd NPs measured by X-ray photoelectron spectroscopy (XPS) spectroscopy.

Sample	BE of Pd $3d_{3/2}$ (eV)		BE of Pt $4f_{7/2}$ (eV)		BE of O 1s (eV)			Pt 4f/Pd 3d
	Pd(0)	Pd(∂+)	Pt(0)	Pt(∂+)	OL	OS	OW	
Pt/TiO_2			71.1 (68) *	73.9 (32) *	530.8 (65) *	532.4 (27) *	534.0 (8)	-
$Pt_{0.50}Pd_{0.50}/TiO_2$	335.8 (77) *	337.4 (23) *	72.4 (85) *	74.3 (15) *	530.8 (63) *	532.8 (30) *	534.9 (7)	1.01
Pd/TiO_2	334.2 (83) *	336.5 (17) *	-	-	530.5 (63) *	532.6 (29) *	534.8 (8)	-
TiO_2	-	-	-	-	530.3 (69) *	532.2 (24) *	534.0 (7)	-

* Atomic percentages of the different Pd, Pt, or O species.

The distribution of oxygen species does not change significantly within the samples. However, differences in the relative ratio of Me^0/Me^{2+} were observed. The interaction between both metals permits us to obtain a higher value of reduced Pt on the surface (Pt^0/Pd^0 = 1.23) as compared to the total Pt/Pd ratio of 1.01 (Table 2).

2.2. Catalytic Tests

As said above, the activities of all prepared catalysts were tested in liquid phase hydrogenation of both glucose and furfural.

2.2.1. Glucose Hydrogenation

The hydrogenation of glucose to sorbitol is generally performed under a high pressure of H_2 to attain high yields. However, in this work, the glucose hydrogenation tests were conducted at relatively low H_2 pressure (15 bar). All samples showed high activities in the hydrogenation of glucose even at this low pressure. At a glucose:metal ratio of 500, complete glucose conversions were obtained for all three catalysts with different compositions: Pt/TiO_2, $Pt_{0.50}Pd_{0.50}/TiO_2$, and Pd/TiO_2. Glucose conversions were reduced to ~50–80% when the glucose:metal ratio increased to 1000. Interesting trends were observed in the sorbitol selectivity results at 80% of glucose iso-conversion, as shown in Figure 5 (glucose:metal ratio of 600). For monometallic catalysts, the sorbitol selectivities varied from 50% to 60%. In contrast, very high sorbitol selectivity of 96% was observed for bimetallic $Pt_{0.50}Pd_{0.50}/TiO_2$ catalysts. Zhang et al. reported that larger nanoparticles of Pt (>17nm) and higher H_2 pressure are necessary to obtain higher sorbitol selectivity on Pt/SBA-15 catalysts [19]. However, we obtained 80% glucose conversion and 92% sorbitol selectivity even with ultra-small particles (<3 nm) at relatively low H_2 pressure (12 bar) using bimetallic catalysts, which once again confirms the possible positive influence of synergy between Pd and Pt metals on the activity of the bimetallic catalyst, no matter how small the particles and hydrogen pressure are. Furthermore, the influence of support TiO_2 cannot be excluded, as it is known to exhibit higher activity than SiO_2 support due to the presence of the strong metal–support interactions (SMSI) phenomenon and O-vacancy on TiO_2 support [52].

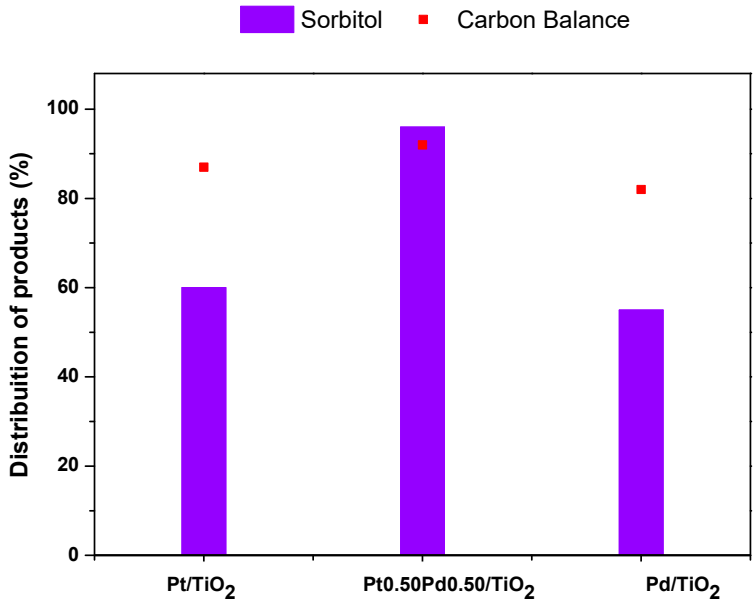

Figure 5. Glucose hydrogenation to sorbitol using Pd, Pt, and PtPd catalysts supported on TiO_2. Distribution of products at glucose iso-conversion of 80%. Conditions: 2 mL of aqueous solution of glucose, 10 mg of catalyst, 2 h, glucose:metal (mol) = 600.

Moreover, the activity was also higher in the case of bimetallic catalysts, compared to their monometallic counterparts. A maximum glucose conversion of 98% was attained with the $Pt_{0.50}Pd_{0.50}/TiO_2$ catalyst. Meanwhile, monometallic Pt/TiO_2 and Pd/TiO_2 catalysts could reach maximum conversions of only 90% and 82%, respectively. These results clearly show that a strong synergistic effect exists between Pt and Pd metals in the bimetallic $Pt_{0.50}Pd_{0.50}/TiO_2$ catalyst. This synergy seems to be correlated to the chemical composition of the bimetallic nanoparticles, with a high content of metallic Pt on the surface as observed from XPS studies.

2.2.2. Furfural Hydrogenation Test

Given the very good performances of the $Pt_{0.50}Pd_{0.50}/TiO_2$ catalyst in glucose hydrogenation, the efficiency of this material in the reductive conversion of another important biomass-based platform chemical (i.e., furfural) was also tested. It has been well established that the partial hydrogenation of furfural leads to the formation of different products, as shown in Figure 6. All these partial hydrogenation products are value-added chemicals that can be used as polymer precursors or solvents [3]. The formation of tetrahydrofurfuryl alcohol (THFA) involves the reduction of the furan ring, which generally requires relatively high hydrogenation activity of the catalyst [3]. The reduction of the aldehyde group of furfural permits the production of furfuryl alcohol (FA), which is used as a green solvent, whereas the hydrogenolysis of the aldehyde group leads to methylfuran (MF), a valuable biofuel [3]. Hence, it is necessary to develop a catalyst which is able to selectively and partially hydrogenate the C=O group without reducing the furan ring in order to produce furfuryl alcohol, one of the many aforementioned hydrogenation products. In this section, the ability of the monometallic and bimetallic catalysts to selectively/partially hydrogenate furfural to furfuryl alcohol will be explored.

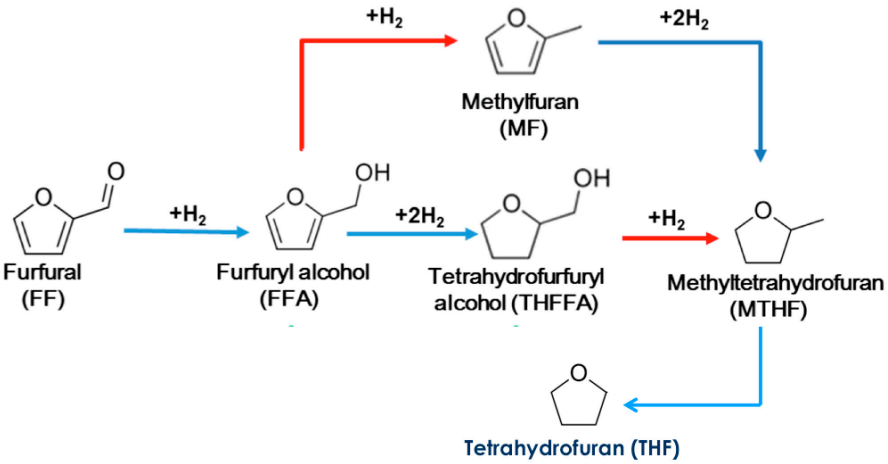

Figure 6. Possible products of the furfural hydrogenation (reprinted from [54]).

It is generally known that solvents have a great influence on the selective distribution of products during liquid hydrogenation of furfural [29]. Hence, the performances of catalysts in furfural hydrogenation were studied in the presence of a protic solvent (isopropanol) and an aprotic solvent (cyclopentyl methyl ether).

The furfural hydrogenation tests were initially performed using isopropanol (protic solvent) as a solvent. The furfural conversions and product distributions obtained on monometallic and bimetallic catalysts are shown in Figure 7.

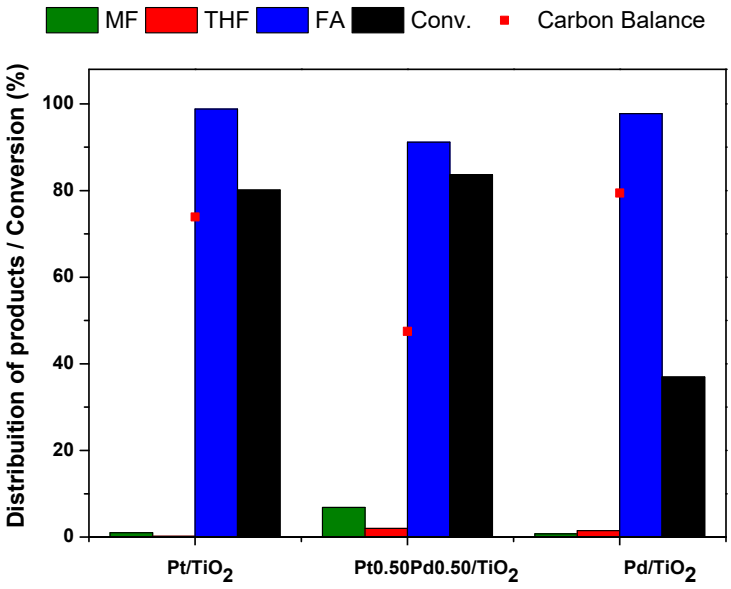

Figure 7. Furfural hydrogenation. Conditions: 2 mL of solution of furfural in isopropanol, 2 h, mass of catalyst = 10 mg, 150 °C, hydrogen pressure of 20 bar, furfural:metal ratio of 10000.

The highest furfural conversion was observed for the bimetallic $Pt_{0.50}Pd_{0.50}/TiO_2$ catalyst (84%). The main product for all catalysts was furfuryl alcohol (FA). However, in the case of the bimetallic catalyst, small amounts of methyl furan (MF) and tetrohydrofuran (THF) were also observed. The main inconvenience in using isopropanol as a solvent is the possibility of forming secondary products (low carbon balance) via catalytic transfer of hydrogen from the solvent [54]. In this case, the ethyl furfuryl ether was formed via a Meerwein–Ponndorf–Verley reaction. This was confirmed in our case by mass spectroscopy. To overcome this issue, new tests were performed using the aprotic solvent cyclopentyl methyl ether (CPME) in order to eliminate etherification and secondary product formation by the transfer of hydrogen. Indeed, when using CPME, the carbon balance reached close to 100%, as can be seen from Figure 8.

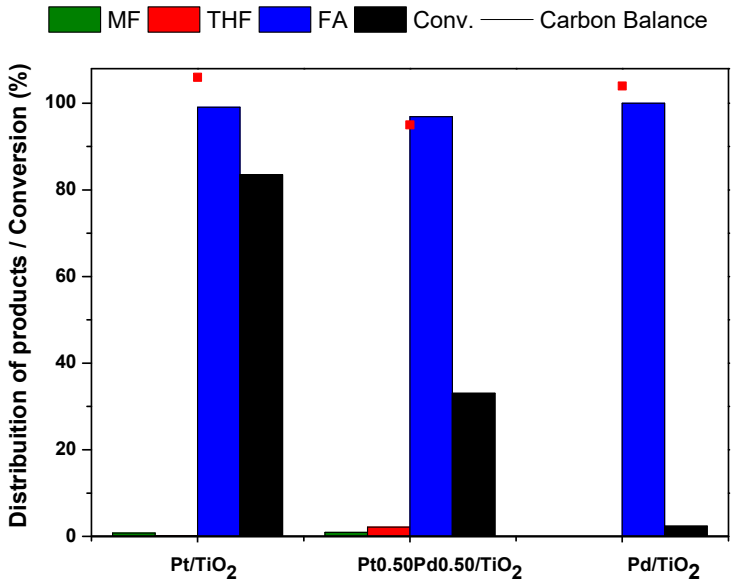

Figure 8. Furfuryl hydrogenation using cyclopentyl methyl ether (CPME) as a solvent. Conditions: 2 mL of solution of furfural in CPME, 2 h, mass of catalyst = 10 mg, 150 °C, hydrogen pressure of 20 bar, furfural:metal ratio of 10000.

All catalysts showed high selectivities to furfuryl alcohol. In the case of the bimetallic sample, a small quantity of THF was also observed. This indicates that the bimetallic sample could perform hydrogenation of the furan ring, which was not observed for pure monometallic samples. The formation of THF required strong reductive properties, as observed for the bimetallic material.

3. Materials and Methods

3.1. Materials

Analytical grade chemicals TiO_2 (P25, titanium oxide, ReagentPlus®, ≥99.5%), NaOH (Sodium hydroxide, 97.0%), HCl (Hydrochloric acid, 37.0%), ethylene glycol (EG, 99.8%), polyvinylpyrrolidone (PVP, M.W. 55,000 g/mol), potassium tetrachloropalladate trihydrate ($K_2PdCl_4 \cdot 3H_2O$, 98%), chloroplatinic acid hexahydrate ($H_2PtCl_6 \cdot 6H_2O$, ≥37.50% Pt basis), L-ascorbic acid ($C_6H_8O_6$, 99%), furfural ($C_5H_4O_2$, > 99%), and glucose (>99%) were used as received. All solutions were prepared using deionized water (18.2 MΩ). All the chemicals were purchased from Sigma-Aldrich, St. Louis, MO, USA.

3.2. Catalyst Preparation

The TiO_2 nanowires were obtained by a hydrothermal method as described below. Firstly, 1 g of TiO_2 (P25 Degussa) was dispersed in 75 mL of 10 M NaOH aqueous solution. The solution was stirred for 30 min at room temperature and then transferred into a Teflon-lined stainless steel autoclave. The autoclave was heated and stirred at 250 °C for 72 h, and then the solution was cooled down to room temperature. The obtained precipitate was added into 500 mL of 0.1 M HCl aqueous solution and stirred. The resulting suspension was centrifuged, and the solid was obtained by decantation of the supernatant. This HCl washing was repeated several times. After HCl washing, the solid was also washed with water several times by successive rounds of centrifugation and removal of the supernatant, until the pH was 7. Titanate wires, obtained by this method, were heated in an air atmosphere at 800 °C for 2 h to produce the TiO_2 nanowires. For the synthesis of TiO_2 nanowires decorated with monometallic Pd or Pt NPs, typically 200 mg of TiO_2 was added to 200 mL of PVP solution (1g/L in EG). The obtained suspension was transferred to a 500 mL round-bottom flask and kept under vigorous stirring at 90 °C for 20 min. Then, 15 mL of 24 mM ascorbic acid aqueous solution and 15 mL of a 24 mM metal precursor solution ($PdCl_4^{2-}{}_{(aq)}$ or $PtCl_6^{2-}{}_{(aq)}$) were sequentially added to the reaction flask. This mixture was kept under vigorous stirring for another 1 h to produce TiO_2–Pd or TiO_2 NPs. For the synthesis of TiO_2 nanowires decorated with monometallic PtPd NPs, the same protocol was employed, but 7.5 mL of each 24 mM metal precursor solution ($PdCl_4^{2-}{}_{(aq)}$ or $PtCl_6^{2-}{}_{(aq)}$) was mixed and added into the system. After the synthesis, the produced nanomaterials were washed three times with ethanol (15 mL) and water (15 mL) by successive rounds of centrifugation at 6000 rpm for 5 min and by the removal of the supernatant. After washing, the nanomaterials were dried at 80 °C under vacuum.

3.3. Catalyst Characterization

The high-resolution transmission electron microscopy (HRTEM) images were obtained with a JEOL JEM2100 microscope (Tokyo, Japan), operated at 200 kV. High-angle annular dark field (HAADF) and energy dispersive x-ray spectroscopy (EDS) images were acquired using a FEI TECNAI G2 F20, operated at 200 kV (Tokyo, Japan). Samples for HRTEM, STEM-HAADF, and STEM-EDX were prepared by drop-casting an aqueous suspension of the nanostructures over a carbon-coated copper grid, followed by drying under ambient conditions. The Pd and Pt atomic percentages were measured by flame atomic absorption spectrometry (FAAS, Tokyo, Japan) with a Shimadzu spectrophotometer (model AA-6300) equipped with an air–acetylene flame. The X-ray diffraction (XRD) data were obtained using a Rigaku-Miniflex equipment (Tokyo, Japan) with CuKα radiation. The diffraction patterns were measured in the range of 0–70°/2θ, with a 1° min^{-1} angular speed scan.

X-ray photoelectron spectroscopy (XPS) data of the samples were obtained on a Kratos Axis Ultra electron spectrometer (Shimadzu, Kyoto, Japan), operating with monochromatic AlKα (1486.6 eV) radiation. The pass energy of the hemispherical analyzer was set to 160 eV for the wide scan and 40 eV for the narrow scan. Peak decomposition was performed using curves with 70% Gaussian type and 30% Lorentzian type, and a Shirley nonlinear sigmoid-type baseline. The binding energies (BE) of the Pd 3d, Pt 4f, Ti 2p, and O 1s spectral peaks were referenced to the C 1s peak at 284.8 eV, providing accuracy within ± 0.1 eV. The samples were thermally treated (under 10% hydrogen, 300 °C for 2 h) in an external reactor coupled to the analysis chamber. This permitted quasi in situ analysis of the catalysts before and after thermal treatment.

Textural characteristics of the catalysts were determined from nitrogen adsorption isotherms, recorded at −196 °C in a Quantachrome Nova 1000 (Boynton Beach, FL, USA). The samples (ca. 100 mg) were degassed for 3 h at 150 °C before analysis. Specific surface areas were determined by the Brunauer–Emmett–Teller equation (BET method) from an adsorption isotherm generated in a relative pressure range $0.07 < P/Po < 0.3$. The total pore volume was calculated from the amount of N_2 adsorbed at a relative pressure close to unity. The average pore diameter was determined by the Barrett–Joyner–Halenda (BJH) method, from the N_2 desorption isotherms.

3.4. Catalytic Tests

Furfural and glucose hydrogenation tests were carried out on the REALCAT platform [22] in a Screening Pressure Reactor system (SPR) from Unchained Labs (London, UK) equipped with 24 parallel batch reactors for high-throughput screening of the catalytic materials.

In the typical glucose hydrogenation reaction, the catalysts (10 mg) were placed in each reactor. Then, 3 mL of an aqueous solution of glucose (1.0 wt.%) were added. The catalytic tests were performed under H_2 (12 bar) for 2 h at 110 °C under non-controlled pH (initial pH = 6). After the reaction, the reactors were cooled down to room temperature. The liquid products were analyzed using High Performance Liquid Chromatography (HPLC, Waters 2410 RJ, Milford, MA, USA) equipped with a Shodex SUGARSH-1011 column (8 × 300 mm) and RI (refractive index) and UV (ultraviolet) detectors. Diluted H_2SO_4 (5 mM, 1 mL/min) was used as a mobile phase. Commercial standards (glucose and sorbitol) were used for calibration of the HPLC setup. Temperature, initial pressure, hydrogen atmosphere, duration of the reaction, catalyst amount, and initial reactant concentration were set as follows: 110 °C, 12 bar, hydrogen, 2 h, glucose:metal ratio of 500:1 (and 600:1). After the first run, the reactant solution was taken out from the reactor using a syringe. The catalyst was recovered by centrifugation, and then dried at 100 °C overnight. The second run was then performed with the same catalyst amounts and conditions as employed during the first run.

Typical furfural hydrogenation tests were performed at 150 °C under 20 bar of H_2 for 2 h. Before reaction, the catalysts (10 mg) were reduced in situ at 400 °C with pure H_2 for 2 h. Then, the furfural solution (2 mL; 25 wt.% in 2-propanol or CPME) was transferred to the reactors inside a glove box. The reactors were then sealed, charged with H_2 (20 bar), and subsequently heated up to 150 °C. The reaction time was initiated after shaking started (600 rpm). Finally, the system was cooled down to room temperature, and the liquid products were analyzed using a GC (Shimadzu GC 2010 PLUS, Kyoto, Japan) equipped with a ZB-WAX Plus column (30 m × 0.25 mm × 0.25 μm) and a FID (flame ionization detector). GC-MS was used to ensure precision in the identification of the products.

The reactant conversions and the distribution of products were calculated on a mole basis as follows:

$$\text{Conversion}(\%) = \frac{\text{mol}^0_{\text{reactant}} - \text{mol}^{\text{end}}_{\text{reactant}}}{\text{mol}^0_{\text{reactant}}} \times 100 \quad (1)$$

$$\text{Distribution of products } (\%) = \frac{\text{mol}_{\text{product}}}{\sum\left(\text{mol}_{\text{all products}}\right)} \times 100 \quad (2)$$

where mol stands for the number of moles of the reactant or products.

4. Conclusions

It was shown that the bimetallic $Pt_{0.50}Pd_{0.50}/TiO_2$ catalyst is a very efficient material for low-pressure hydrogenation of glucose and furfural reactions. A correlation between the catalytic results obtained and the physicochemical properties of the supported nanoparticles allowed for the identification of key factors responsible for the synergetic behavior of the PtPd system. The high activity and selectivity exhibited by the bimetallic PtPd catalyst was due to the ultra-small particle sizes, alloy formation, and specific Pt-rich composition of the bimetallic particles supported on the TiO_2 nanowires. The catalytic activity of Pt-based materials in the liquid phase hydrogenation reactions of glucose and furfural significantly increased when the reduced Pt was located on the catalyst surface. Besides, the PtPd material with finely dispersed bimetallic particles showed high potential in the reductive transformation of furfural to value-added furfuryl alcohol. This study provides new insights into how the interaction between two metals can be explored to obtain highly active Pt-based NPs that act as excellent catalysts for liquid phase hydrogenation reactions.

Author Contributions: R.W., P.M.d.S., L.S., A.G.M.d.S., C.G.F., and T.S.R. conceived and designed the experiments; A.G.M.d.S. and P.M. performed the experiments; R.W., P.H.C.C., S.P., and T.S.R. analyzed the data; all the authors contributed to the writing of the paper.

Funding: This work was done in the frame of the LIA "Energy&Environment" funded by CNRS. The authors acknowledge support from FAPESP (Grant numbers No. 2015/50010-8, 15/26308-7, and 2017/03235-0).

Acknowledgments: The REALCAT platform is benefiting from a state subsidy administrated by the French National Research Agency (ANR) within the frame of the 'Investments for the Future' program (PIA), with the contractual reference 'ANR-11-EQPX-0037'. The European Union, through the ERDF funding administered by the Hauts-de-France Region has co-financed the platform. Centrale Lille, CNRS, and the University of Lille, as well as the Centrale Initiatives Foundation, are thanked for their financial contributions to the acquisition and implementation of the equipment of the REALCAT platform.

Conflicts of Interest: The authors declare no conflict of interest.

References

1. Climent, M.J.; Corma, A.; Iborraa, S. Conversion of biomass platform molecules into fuel additives and liquid hydrocarbon fuels. *Green Chem.* **2014**, *16*, 516–547. [CrossRef]
2. Li, X.; Jia, P.; Wang, T. Furfural: A Promising Platform Compound for Sustainable Production of C4 and C5 Chemicals. *ACS Catal.* **2016**, *6*, 7621–7640. [CrossRef]
3. Chen, S.; Wojcieszak, R.; Dumeignil, F.; Marceau, E.; Royer, S. How Catalysts and Experimental Conditions Determine the Selective Hydro conversion of Furfural and 5-Hydroxymethylfurfural. *Chem. Rev.* **2018**, *118*, 11023–11117. [CrossRef] [PubMed]
4. Climent, M.J.; Corma, A.; Iborraa, S. Converting carbohydrates to bulk chemicals and fine chemicals over heterogeneous catalysts. *Green Chem.* **2011**, *13*, 520–540. [CrossRef]
5. Ahmed, M.J.; Hameed, B.H. Hydrogenation of glucose and fructose into hexitols over heterogeneous catalysts: A review. *J. Taiwan Inst. Chem. Eng.* **2018**. [CrossRef]
6. Bozell, J.J.; Petersen, G.R. Technology development for the production of biobased products from biorefinery carbohydrates—The US Department of Energy's "Top 10" revisited. *Green Chem.* **2010**, *12*, 539–554. [CrossRef]
7. Marques, C.; Tarek, R.; Sara, M.; Brar, S.K. Sorbitol Production from Biomass and Its Global Market. In *Platform Chemical Biorefinery*; Brar, S.K., Sarma, S.J., Pakshirajan, K., Eds.; Elsevier: Amsterdam, The Netherlands, 2016; pp. 217–227, ISBN 9780128029800.
8. Eseyin, A.E.; Steele, P.H. An overview of the applications of furfural and its derivatives. *Int. J. Adv. Chem.* **2015**, *3*, 42–47. [CrossRef]
9. Takagaki, A.; Nishimura, S.; Ebitani, K. Catalytic Transformations of Biomass-Derived Materials into Value-Added Chemicals. *Catal. Surv. Asia* **2012**, *16*, 164–182. [CrossRef]
10. Gupta, K.; Rai, R.K.; Singh, S.K. Metal Catalysts for the Efficient Transformation of Biomass-derived HMF and Furfural to Value Added Chemicals. *ChemCatChem* **2018**, *10*, 2326–2349. [CrossRef]

11. Gorp, K.; Boerman, E.; Cavenaghi, C.V.; Berben, P.H. Catalytic hydrogenation of fine chemicals: Sorbitol production. *Catal. Today* **1999**, *52*, 349–361. [CrossRef]
12. Hoydonckx, H.E.; Van Rhijn, W.M.; Van Rhijn, W.; De Vos, D.E.; Jacobs, P.A. Furfural and Derivatives. In *Ullmann's Encyclopedia of Industrial Chemistry*; Wiley-VCH Verlag GmbH & Co.: Weinheim, Germany, 2007. [CrossRef]
13. Romero, A.; Nieto-Márquez, A.; Alonso, E. Bimetallic Ru:Ni/MCM-48 catalysts for the effective hydrogenation of d-glucose into sorbitol. *Appl. Catal. A Gen.* **2017**, *529*, 49–59. [CrossRef]
14. Romero, A.; Alonso, E.; Sastre, A.; Nieto-Márquez, A. Conversion of biomass into sorbitol: Cellulose hydrolysis on MCM-48 and d-Glucose hydrogenation on Ru/MCM-48. *Microporous Mesoporous Mater.* **2016**, *224*, 1–8. [CrossRef]
15. Mishra, D.K.; Lee, J.-M.; Chang, J.-S.; Hwang, J.S. Liquid phase hydrogenation of d-glucose to d-sorbitol over the catalyst (Ru/NiO–TiO_2) of ruthenium on a NiO-modified TiO_2 support. *Catal. Today* **2012**, *185*, 104–108. [CrossRef]
16. Bizhanov, F.B.; Sokolskiy, D.V.; Popov, N.I.; Malkina, N.Y.; Khisametdinov, A.M. Hydrogenation of glucose on Raney nickel. I. *J. Catal.* **1968**, *10*, 206–207. [CrossRef]
17. Negoi, A.; Triantafyllidis, K.; Parvulescu, V.I.; Coman, S.M. The hydrolytic hydrogenation of cellulose to sorbitol over M (Ru, Ir, Pd, Rh)-BEA-zeolite catalysts. *Catal. Today* **2014**, *223*, 122–128. [CrossRef]
18. Lazaridis, P.A.; Karakoulia, S.; Delimitis, A.; Coman, S.M.; Parvulescu, V.I.; Triantafyllidis, K. D-Glucose hydrogenation/hydrogenolysis reactions on noble metal (Ru, Pt)/activated carbon supported catalysts. *Catal. Today* **2015**, *257*, 281–290. [CrossRef]
19. Zhang, X.; Durndell, L.J.; Isaacs, M.A.; Parlett, C.M.A.; Lee, A.F.; Wilson, K. Platinum-Catalyzed Aqueous-Phase Hydrogenation of D-Glucose to D-Sorbitol. *ACS Catal.* **2016**, *6*, 7409–7417. [CrossRef]
20. Baijun, L.; Lianhai, L.; Bingchun, W.; Tianxi, C.; Iwatani, K. Liquid phase selective hydrogenation of furfural on Raney nickel modified by impregnation of salts of heteropolyacids. *Appl. Catal. A Gen.* **1998**, *171*, 117–122. [CrossRef]
21. Merat, N.; Godawa, C.; Gaset, A. High Selective Production of Tetrahydrofurfuryl Alcohol: Catalytic Hydrogenation of Furfural and Furfuryl Alcohol. *J. Chem. Technol. Biotechnol.* **1990**, *48*, 145–159. [CrossRef]
22. Li, H.; Luo, H.; Zhuang, L.; Dai, W.; Qiao, M. Liquid phase hydrogenation of furfural to furfuryl alcohol over the Fe-promoted Ni-B amorphous alloy catalysts. *J. Mol. Catal. A Chem.* **2003**, *203*, 267–275. [CrossRef]
23. Neill, B.J.O.; Jackson, D.H.K.; Crisci, A.J.; Farberow, C.A.; Shi, F.; Alba-Rubio, A.C.; Lu, J.; Dietrich, P.J.; Gu, X.; Marshall, C.L.; et al. Stabilization of Copper Catalysts for Liquid-Phase Reactions by Atomic Layer Deposition. *Angew. Chem. Int. Ed.* **2013**, *52*, 13808–13812. [CrossRef] [PubMed]
24. Vargas-Hernandez, D.; Rubio-Caballero, J.M.; Santamaria-Gonzalez, J.; Moreno-Tost, R.; Merida-Robles, J.M.; Perez-Cruz, M.A.; Jimenez-Lopez, A.; Hernandez-Huesca, R.; Maireles-Torres, P. Furfuryl alcohol from furfural hydrogenation over copper supported on SBA-15 silica catalysts. *J. Mol. Catal. A Chem.* **2014**, *383–384*, 106–113. [CrossRef]
25. Rao, R.; Dandekar, A.; Baker, R.T.K.; Vannice, M.A. Properties of Copper Chromite Catalysts in Hydrogenation Reactions. *J. Catal.* **1997**, *171*, 406–419. [CrossRef]
26. Huang, R.; Cui, Q.; Yuan, Q.; Wu, H.; Guan, Y.; Wu, P. Total hydrogenation of furfural over Pd/Al_2O_3 and Ru/ZrO_2 mixture under mild conditions: Essential role of tetrahydrofurfural as an intermediate and support effect. *ACS Sustain. Chem. Eng.* **2018**, *6*, 6957–6964. [CrossRef]
27. Scholz, D.; Aellig, C.; Hermans, I. Catalytic Transfer Hydrogenation/Hydrogenolysis for Reductive Upgrading of Furfural and 5-(Hydroxymethyl)furfural. *ChemSusChem* **2014**, *7*, 268–275. [CrossRef] [PubMed]
28. Fulajtárova, K.; Soták, T.; Hronec, M.; Vávra, I.; Dobroˇcka, E.; Omastová, M. Aqueous phase hydrogenation of furfural to furfuryl alcohol over Pd–Cu catalysts. *Appl. Catal. A Gen.* **2015**, *502*, 78–85. [CrossRef]
29. Taylor, M.J.; Durndell, L.J.; Isaacs, M.A.; Parlett, C.M.A.; Wilson, K.; Lee, A.F.; Kyriakou, G. Highly selective hydrogenation of furfural over supported Pt nanoparticles under mild conditions. *Appl. Catal. B* **2016**, *180*, 580–585. [CrossRef]
30. An, K.; Musselwhite, N.; Kennedy, G.; Pushkarev, V.V.; Baker, L.R.; Somorjai, G.A. Preparation of mesoporous oxides and their support effects on Pt nanoparticle catalysts in catalytic hydrogenation of furfural. *J. Colloid Interface Sci.* **2013**, *392*, 122–128. [CrossRef]

31. Liu, L.; Lou, H.; Chen, M. Selective hydrogenation of furfural over Pt based and Pd based bimetallic catalysts supported on modified multi walled carbon nanotubes (MWNT). *Appl. Catal. A Gen.* **2018**, *550*, 5–10. [CrossRef]
32. Merlo, A.B.; Vetere, V.; Ruggera, J.F.; Casella, M.L. Bimetallic PtSn catalyst for the selective hydrogenation of furfural to furfuryl alcohol in liquid-phase. *Catal. Lett.* **2009**, *10*, 1665–1669. [CrossRef]
33. Arena, B.J. Deactivation of ruthenium catalysts in continuous glucose hydrogenation. *Appl. Catal. A Gen.* **1992**, *87*, 219–229. [CrossRef]
34. Kusserow, B.; Schimpf, S.; Claus, P. Hydrogenation of Glucose to Sorbitol over Nickel and Ruthenium Catalysts. *Adv. Synth. Catal.* **2003**, *345*, 289–299. [CrossRef]
35. Liu, D.; Zemlynov, D.; Wu, T.; Lobo-Lapidus, R.J.; Dumesic, J.A.; Miller, J.T.; Marshall, C.L. Deactivation mechanistic studies of copper chromite catalyst for selective hydrogenation of 2-furfuraldehyde. *J. Catal.* **2013**, *299*, 336–345. [CrossRef]
36. Rodiansono; Khairi, S.; Hara, T.; Ichikuni, N.; Shimazu, S. Highly efficient and selective hydrogenation of unsaturated carbonyl compounds using Ni–Sn alloy catalysts. *Catal. Sci. Technol.* **2012**, *2*, 2139–2145.
37. Twigg, M.V.; Spencer, M.S. Deactivation of supported copper metal catalysts for hydrogenation reactions. *Appl. Catal. A Gen.* **2001**, *212*, 161–174. [CrossRef]
38. Morales-Torres, S.; Carrasco-Marín, F.; Pérez-Cadenas, A.F.; Maldonado-Hódar, F.J. Coupling Noble Metals and Carbon Supports in the Development of Combustion Catalysts for the Abatement of BTX Compounds in Air Streams. *Catalysts* **2015**, *5*, 774–799. [CrossRef]
39. Muroi, T. Role of Precious Metal Catalysts. In *Noble Metals*; Su, Y.-H., Ed.; InTechOpen Limited: London, UK, 2012; ISBN 978-953-307-898-4.
40. Basile, F.; Basini, L.; Fornasari, G.; Gazzano, M.; Trifiro, F.; Vaccari, A. Anionic Clays as Precursors of Noble Metal Based Catalysts for Methane Activation. *Stud. Surf. Sci. Catal.* **1998**, *118*, 31–40.
41. Sitthisa, S.; Pham, T.; Prasomsri, T.; Sooknoi, T.; Mallinson, R.G.; Resasco, D.E. Conversion of furfural and 2-methylpentanal on Pd/SiO_2 and $Pd–Cu/SiO_2$ catalysts. *J. Catal.* **2011**, *280*, 17–27. [CrossRef]
42. Nakagawa, Y.; Takada, K.; Tamura, M.; Tomishige, K. Total Hydrogenation of Furfural and 5-Hydroxymethylfurfural over Supported Pd−Ir Alloy Catalyst. *ACS Catal.* **2014**, *4*, 2718–2726. [CrossRef]
43. Liu, C.; Zhang, C.; Liu, K.; Wang, Y.; Fan, G.; Sun, S.; Xu, J.; Zhu, Y.; Li, Y. Aqueous-phase hydrogenolysis of glucose to value-added chemicals and biofuels: A comparative study of active metals. *Biomass Bioenergy* **2015**, *72*, 189–199. [CrossRef]
44. Pino, N.; Sitthisa, S.; Tan, Q.; Souza, T.; López, D.; Resasco, D.E. Structure, activity, and selectivity of bimetallic $Pd-Fe/SiO_2$ and $Pd-Fe/\gamma-Al_2O_3$ catalysts for the conversion of furfural. *J. Catal.* **2017**, *350*, 30–40. [CrossRef]
45. Albertazzi, S.; Busca, G.; Finocchio, E.; Glöckler, R.; Vaccari, A. New Pd/Pt on Mg/Al basic mixed oxides for the hydrogenation and hydrogenolysis of naphthalene. *J. Catal.* **2004**, *223*, 372–381. [CrossRef]
46. Gomez, R.; Angel, G.D.; Damian, C.; Corro, G. Platinum-palladium catalysts in hydrogenation of methylbenzenes. *React. Kinet. Catal. Lett.* **1979**, *11*, 137–142. [CrossRef]
47. Rousset, J.L.; Stievano, L.; Aires, F.J.C.S.; Geantet, C.; Renouprez, A.J.; Pellarin, M. Hydrogenation of Toluene over γ-Al2O3-Supported Pt, Pd, and Pd–Pt Model Catalysts Obtained by Laser Vaporization of Bulk Metals. *J. Catal.* **2001**, *197*, 335–343. [CrossRef]
48. Shafii, S.; Lihua, W.; Nordin, M.R.; Yong, L.K. Synthesis of Palladium-Platinum Bimetallic Nanoparticles and their Catalytic Activity towards the Hydrogenation Reaction of Palm Olein. *J. Chem. Eng. Process Technol.* **2012**, *3*, 1–8. [CrossRef]
49. Baldovino-Medrano, V.G.; Pollefeyt, G.; Bliznuk, V.; Van Driessche, I.; Gaigneaux, E.M.; Ruiz, P.; Wojcieszak, R. Synergetic Behavior of TiO_2-Supported Pd(z)Pt(1-z)Catalysts in the Green Synthesis of Methyl Formate. *ChemCatChem* **2016**, *8*, 1–11. [CrossRef]
50. Albilali, R.; Douthwaite, M.; He, Q.; Taylor, S.H. The selective hydrogenation of furfural over supported palladium nanoparticle catalysts prepared by sol-immobilisation: Effect of catalyst support and reaction conditions. *Catal. Sci. Technol.* **2018**, *8*, 252–267. [CrossRef]
51. Geyer, R.; Kraak, P.; Pachulski, A.; Schodel, R. New Catalysts for the Hydrogenation of Glucose to Sorbitol. *Chem. Ing. Tech.* **2012**, *84*, 513–516. [CrossRef]

52. Baker, L.R.; Kennedy, G.; Spronsen, M.V.; Hervier, A.; Cai, X.; Chen, S.; Wang, L.-W.; Somorjai, G.A. Furfuraldehyde Hydrogenation on Titanium Oxide-Supported Platinum Nanoparticles Studied by Sum Frequency Generation Vibrational Spectroscopy: Acid−Base Catalysis Explains the Molecular Origin of Strong Metal−Support Interactions. *J. Am. Chem. Soc.* **2012**, *134*, 14208–14216. [CrossRef]
53. Fuentes Hernandez, A.; Lee, R.; Beland, N.; Zamboni, I.; Lavoie, J.M. Reduction of Furfural to Furfuryl Alcohol in Liquid Phase over a Biochar-Supported Platinum Catalyst. *Energies* **2017**, *10*, 286. [CrossRef]
54. Shi, D.; Yang, Q.; Peterson, C.; Lamic-Humblot, A.-F.; Girardon, J.-S.; Griboval-Constant, A.; Stievano, L.; Sougrati, M.T.; Briois, V.; Bagot, P.; et al. Bimetallic Fe-Ni/SiO_2 catalysts for furfural hydrogenation: Identification of the interplay between Fe and Ni during deposition-precipitation and thermal treatments. *Catal. Today* **2018**. [CrossRef]
55. Wojcieszak, R.; Zielinski, M.; Monteverdi, S.; Bettahar, M. Study of nickel nanoparticles on activated carbon prepared by aqueous hydrazine reduction. *J. Coll. Inter. Sci.* **2006**, *299*, 238. [CrossRef] [PubMed]